Flexographic Printing – Towards an advanced front side metallization approach with high throughput and low silver consumption

A. Lorenz[1], C. Gredy[1], S. Beyer[2], Y. Yao[3], P. Papet[3], J. Ufheil[2], A. Senne[4], H. Reinecke[5], F. Clement[1]

[1]Fraunhofer Institute for Solar Energy Systems (ISE), Heidenhofstrasse 2, 79110 Freiburg

[2]Somont GmbH, Im Brunnenfeld 8, 79224 Umkirch, Germany

[3]Meyer Burger AG, Schorenstrasse 39, CH-3645 Gwatt

[4]ContiTech Elastomer-Beschichtungen GmbH, Breslauer Str. 14, 7154 Northeim, Germany

[5]Albert-Ludwigs-Universität, Institut für Mikrosystemtechnik, Georges-Köhler-Allee 101, 79110 Freiburg, Germany

Corresponding Author : Andreas Lorenz, Fraunhofer ISE, Heidenhofstr. 2, 79110 Freiburg, Germany, Phone: +49-761-4588-5299, E-Mail: andreas.lorenz@ise.fraunhofer.de

ABSTRACT

Rotational flexographic printing technology is a highly promising approach to increase the productivity of the cost-intensive solar cell metallization process. The ability to realize narrow contact fingers with very low silver consumption makes this technology particularly attractive for the front side metallization of busbarless solar cells in combination with multi-wire interconnection like Meyer Burger's SmartWire Connection Technology (SWCT). Within this work, we investigate the feasibility of this approach on solar cells with 156 mm edge length. Two types of silver inks are prepared and evaluated with focus on optical and electrical properties of the printed front side grid. Both inks achieve sufficient lateral finger resistances below 20 Ω/cm. A low specific contact resistance of $\rho_{c,95\%} = 3.0 \pm 0.6$ mΩcm² is obtained with ink A. Using flexographic printing, Aluminium back surface field Czrochalski-grown Silicon busbarless solar cells with a maximum conversion efficiency of η = 19.4 % ($\eta_{\varnothing}$ = 19.0 %) are fabricated and interconnected to a mini-module. The mini-module obtains an aperture conversion efficiency of η = 15.8 %. The origin of the cell-to-module (CTM) losses are examined in detail. It is shown that a certain part of the CTM-losses originates from the characteristics of the used Grid^{TOUCH} I-V-measurement device. Further sources of possible CTM losses are investigated using electroluminescence measurement (EL) and discussed in detail.

Keywords: Rotational printing technology; Flexographic Printing; SmartWire Connection Technology; multi-wire interconnection; Busbarless Solar Cells

1. Introduction

To date, screen printing is the common technique for solar cell front and rear side metallization. However, this technology has some drawbacks – namely the limitation of throughput and the incapability to print very narrow lines with low silver consumption. A variety of alternative printing technologies like aerosol printing [1,2], inkjet [3,4], fine line screen printing [5,6], gravure [7] and others have been deeply investigated to overcome these drawbacks. Yet, an alternative technology can only prevail if it combines several requirements like high productivity, easy handling, high reliability and the possibility to use commercially available consumables (inks, printing forms etc.). Rotational flexographic printing is a very promising technology which meets these challenging demands. This printing technology is widely used in graphic arts printing on substrates like cardboard, paper or foil. Such printing machines can realize a printing speed of up to 800 m/min. on web based materials. However, this throughput can not be realized for non-continous printing on Si wafers. A single metallization line using rotational printing is expected to enable a throughput of 3000 to 5000 wafers/h which would be considerably higher than modern screen printing lines with approx. 2000 wafers/h. Fig. 1 illustrates the working principle of a flexographic printing unit for solar cell metallization.

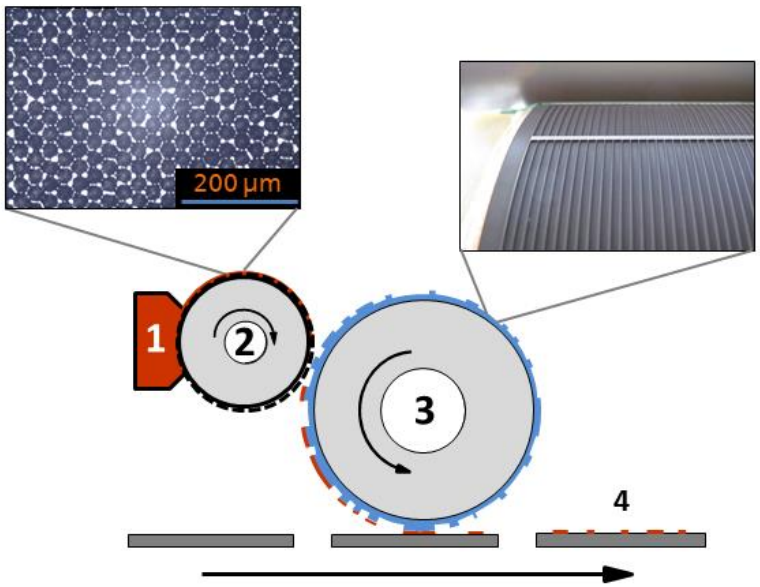

Fig. 1. Schematic drawing of a flexographic printing platform for silicon solar cells: From the ink reservoir (1), a defined amount of ink is transferred by the anilox roll (2) onto fine finger elements on the printing plate (3) and the silicon wafer (4).

A flexible relief printing plate is used as image carrier. Compressible foam tape is applied below the printing plate to support a homogeneous ink transfer. Low-viscous ink is transferred from the ink chamber onto the so-called anilox roll, a steel cylinder with a finely textured chromium or ceramic surface. Excessive ink is removed by a doctor blade before the anilox roller wets the elevated areas of the printing plate with a uniform layer thickness and directly prints the elevated printing image on the substrte. The flexible printing plate and the relatively low printing pressure enable a homogeneous and precise printing quality even on very rough substrates like textured silicon wafers.

Flexographic printing, also known as flexography or flexo, has already proven its ability to print ultrafine conductive structures in many printed electronics applications like micro-scale conductive networks [8,9], roll-to-roll polymer solar cell modules [10], cathode layers for batteries [11] or conductive lines [12]. Feasibility studies using flexography on small-sized solar cell samples have demonstrated the potential of this technology to realize ultrafine contact fingers [13–15]. Conversion efficiencies up to η = 18.8 % have been demonstrated for flexo-printed silicon solar cells using a seed and plate approach [16].

The interconnection of conventional H-pattern solar cells by stringing the cells with soldered ribbons on printed busbars causes significant electrical losses which limit the power output of the module. An innovative approach to overcome this drawback is the interconnection of busbarless solar cells by wire-bonding of multiple thin wires on the front side grid. Meyer Burger's Smart Wire Connection Technology (SWCT) is a very promising approach to realize this concept on an industrial base [17]. Busbarless solar cells with a front side grid consisting only of contact fingers are interconnected by 15 to 38 round copper wires. Typically, 18 wires with a diameter of d_{wire} = 200 µm are used for interconnection. The wires are coated with a low-melting alloy including 50 % Indium [17]. The amount and thickness of the wires can be customized depending on the properties of the solar cell front side metallization. The wires are embedded in a PET foil, the so-called foil-wire electrode (FWE). The FWE is laminated with a certain pressure and temperature directly onto the front and rear side of the solar cells. SWCT offers the potential to reduce costs and raise module efficiency considerably due to several benefits. Ohmic power losses of the front side grid can be reduced due to significantly smaller finger segment lengths in between the wires. Silver consumption is considerably smaller due to the lack of printed busbars and the possibility to print smaller fingers. Light coupling into the module is increased due to a better back-reflection behavior of the round-shaped wires. The passivation quality of the rear side is increased as no silver solder pads are needed. Finally, the impact of cell breakage is considerably smaller due to multiple current

collection pathways [17]. A detailed feasibility study has shown that flexographic printing is a highly interesting for the front side metallization of busbarless solar cells [18]. Within this work, we demonstrate the first busbarless solar cells with flexo-printed front side metallization and a fully functional mini-module with SWCT interconnection.

2. Experiment

2.1 Wafer material

The experiment is carried out using industrially pre-produced Czrochalski-grown Silicon (Cz-Si) p-type solar cells up to anti-reflection coating (precursors) with an edge length of 156 mm. The precursors have a p-type base resistivity of approx. $\rho_b \approx 2.8 - 3.3$ Ωcm and a n-type phosphorous doped emitter with a sheet resistance of $R_{sh} \approx$ 85-90 Ω/sq. The front side is textured by alkaline wet chemical etching and coated with SiN_x anti-reflection coating (ARC) by plasma-enhanced chemical vapour deposition (PECVD). The rear side of the cells is metallized with screen printed aluminum paste to form the back surface field (Al BSF) after contact firing.

2.2 Printing Platform

A roll-to-flat flexographic printing platform *Nissha Angstromer S15* is used to apply the front side metallization of the solar cells (Fig. 2). This machine has a vacuum substrate holder to fix the wafer during the printing process. The position of the vacuum substrate holder perpendicular to the axis of the printing cylinder (*z*-position) is adjusted by a micrometer spindle. A tri-helical engraved anilox roll with a screening of 119 lines/cm and a nominal dip volume of V_D = 7.2 cm³/m² is used to transfer a constant amount of silver ink on the printing plate. The ink is applied by a pipette directly on the anilox roller. A steel doctor blade removes the excessive ink from the anilox roll.

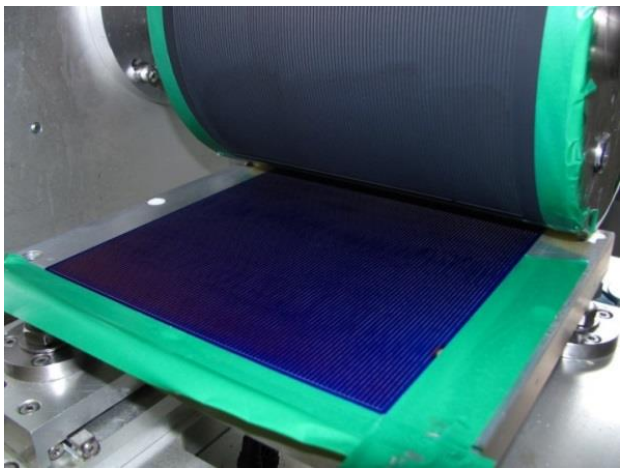

Fig. 2. Flexographic printing platform used for the experiment

A double printing step with an intermediate drying step using an industrial heating blower is applied on the front side of the precursors. The register accuracy between the two printing steps on the used machine is estimated with approx. ± 5 µm as the wafer is constantly fixed by vacuum during the whole procedure. For an industrial application of this process, it would thus be necessary to realize a serial arrangement of two printing units with a register accuracy of ± 10 µm or better. In contrary to a previous experiment [19], several process optimizations are applied. Instead of a hard substructure under the printing plate, a stack of soft foam tapes is used. It is anticipated that this softer substructure helps to reduce the deformation of the finger elements on the plate under pressure and thus prevents excessive spreading of the ink. Secondly, an new ink formulation with a higher viscosity is used. Thirdly, an optimized three-dimensional shape of the contact fingers on the laser-engraved elastomeric plate is realized. Finally, the anilox roll, printing cylinder and vacuum substrate holder is adjusted precisely using *Fujifilm Prescale LLLW* pressure-sensitive films.

2.3 Fabrication of solar cells with flexo-printed front side grid

60 Cz-Si precursors with screen-printed Al rear side metallization to form an Al BSF are metallized on the front side with aflexo-printed front side grid (100 contact fingers) using two types of silver based inks (Ag-inks). Ink A is developed in-house and contains silver particles for metal-semiconductor contact formation, lead glass as a sintering additive, solvents, synthetic resin as binder and further additives to adjust viscosity, dispersion and electrical contact formation to the emitter. The formulation of this ink is based on a previously developed aerosol jet ink [2] and has been iteratively optimized for flexographic printing within several previous experiments [16,19,20]. Ink B is a state-of-the-art screen printing Ag-

paste for solar cell front side metallization which is diluted to an adequate dynamic viscosity η for flexographic printing. The dynamic viscosity depending on the shear rate $\eta(\dot{\gamma})$ of both inks is analyzed using an *Anton Paar MCR 101* rheometer with a cone-plate-setup (d = 25 mm, α = 1°).

The flexo-printed front side metallization is carried out using a *ContiTech Laserline CSC* flexo printing plate. A double printing step with intermediate drying is carried out on each wafer to increase the contact finger height. Printing parameters are kept constant for both inks. All solar cells are cured in a *Heraeus* cabinet dryer directly after printing. Subsequently, a contact firing variation at three temperatures (T_1 = 880°C, T_2 = 900°C, T_3 = 920°C) is carried out. Finally, I-V-curves of all fabricated solar cells are measured using a Pasan Spot$^{\text{LIGHT}}$-system with a Grid$^{\text{TOUCH}}$ measuring unit (see section 2.5).

2.4 Evaluation of two silver inks

In order to investigate the performance of both silver inks, a profound characterization of the printed and fired front side grids with focus on the optical and electrical performance is carried out. Mean finger width w_f is measured at 5 identical positions on 10 wafers per group using an *Olympus Lext* confocal microscope (amplification factor 500x), resulting in approx. 50 measurements per group. To ensure an objective evaluation and comparison of the finger width, the microscopic images are analyzed using the image analysis algorithm *SpotLob V6* which has been developed at *Fraunhofer ISE*.

Two parameters are of particular importance to assess the electrical performance of the Ag-inks: Specific contact resistance ρ_c is primarily influenced by the ink properties, the firing conditions and the emitter. Mean lateral finger resistance R_L mainly depends on the contact finger shape (conduction-relevant cross-section), the sintering properties of the ink and the firing conditions. With regard to a low series resistance contribution, both parameters should be as low as possible. Especially realizing a low R_L could be a particular challenge for flexographic printing due to the low amount of transferred ink. Furthermore, a narrow mean contact finger width w_f is of importance to minimize shading losses and thus ensure a high short-circuit current density j_{sc}.

To determine R_L, absolute finger resistance R_f is measured on cut-out samples of several solar cells per group (3 contact fingers on each sample) using four-point measurement method. 17 to 19 individual measurements are carried out in total per group. Subsequently, lateral finger resistance per unit length R_L [Ω/cm] is calculated with the known distance of the

measurement pins (d = 23 mm). Specific contact resistance ρ_c is measured using transfer length method (TLM) [21]. TLM requires contact fingers with a low lateral resistance and an adequate finger height to ensure a good contact of the measuring pins to the contact fingers. Therefore, all TLM samples are reinforced using silver light-induced plating (Ag-LIP) beforehand. It should thus be considered that the plating step might have a positive impact on contact formation, resulting in lower contact resistance values [22]. Five TLM samples are cut out from two selected solar cells of each group. The average specific contact resistance ρ_c is calculated as a mean value of these five measurements.

2.5. Characteristics of the IV-measurement system

To date, the electrical characterization of busbarless solar cells is still challenging as standard flash testers usually contact the printed and fired busbars on the solar cells. To meet this special challenge, the Grid^{TOUCH}-System has been recently developed by Pasan S.A. Grid^{TOUCH} is a contacting unit specially designed for busbarless solar cells and can be used with cell testers from the Spot^{LIGHT} family [23]. The Grid^{TOUCH}-unit consists of an upper and lower set of 30 parallel wires (diameter d_{wire} = 300 µm) which are oriented perpendicular to the fingers of the front side grid. Thus, the measurement setup for the solar cells is fundamentally different to the interconnection in the module where the FWE typically contains 18 wires with a diameter of d_{wire} = 200 µm. During the measurement, the wires of the Grid^{TOUCH} unit contact the fingers on the front side and the aluminum back electrode on the rear side with a certain pressure. Current and voltage is measured under illumination with an AM1.5 spectrum.. By adjusting the light intensity based on a previous calibration, the effective j_{sc} of the bare busbarless solar cell is determined without shading influence of the contacting wires. Within the module, j_{sc} is obviously lower due to the shading impact of the wires. Consequently, one can expect a considerable j_{sc}-offset between the I-V-measurement of the busbarless solar cells using the Grid^{TOUCH}/ Spot^{LIGHT}-system (GT/SL) and the I-V-results of a module using the same solar cells.

Furthermore, it has to be considered that GT/SL determines the *FF* based on a measurement with 30 wires and a mechanical pressure contact. Within the module, the solar cells are typically interconnected by 18 wires using a wire-bonding process. A high R_L of the fingers will thus induce a considerably higher R_s-contribution of the grid due to increased finger segment lengths. A previous study has shown that the different R_s-contribution of the grid can be neglected for typical screen printed fingers with a very low R_L [24]. Yet, the impact of R_L cannot be neglegted for flexo printed contact fingers with a high R_L. The impact of the

different contacting mechanism between wires and fingers in GT/SL and module is yet unknown and might be considerably different for fingers with a low height. Interconnecting such solar cells with more or less than 30 wires consequently evokes a considerable *FF*-offset between GT/SL-values and I-V-values of the module.

2.6 Fabrication and evaluation of a wire-interconnected mini-module

Two busbarless solar cells of group A with the highest conversion efficiency η are interconnected via SWCT using a standard FEW with 18 wires. The FWE is laminated onto the solar cell surface at a temperature of T = 145°C. The wire-bonding process forms the electrical contact between the front side metallization and the interconnecting wires. Subsequently, the interconnected solar cell string is laminated to a mini-module using thermoplastic polyolefin (TPO) encapsulant, back sheet material, crosslinking ribbons and glass (Fig. 3). The I-V-results of the mini-module are measured at Fraunhofer ISE Callab using a Pasan MFG 502 SunSim3BM PAA0571 measuring device with standard conditions (AM1.5 spectrum, Irridation 999.2 W/m²). The measurement is carried out with a black mask with an opening area of 318 mm x 158 mm (area of solar cells with a surrounding edge of approx. 1 mm width). Thus, the conversion efficency of the mini-module represents the aperture area conversion efficiency, meaning that the I-V-results are related to the area of the solar cells plus a small edge zone around the cells. An electroluminscence measurement (EL) of the module is carried out with I = 4A and t = 1500 ms.

Fig. 3. Fabricated mini-module using two flexo printed solar cells of group A with SmartWire-interconnection (18 wires).

3. Results and discussion

3.1. Evaluation of Ag-inks

Fig. 5 shows the mean finger width w_f of the solar cells printed with ink A (Group A) and B (Group B). Group A achieved an average finger width of $w_{f,95\%}$= 55 µm ± 2 µm (95% confidence interval) with a standard deviation of s = 7 µm. The finger widths of both groups are normally distributed, all measured individual values are within a variation of ± 3σ (Fig. 4). Group B obtained a mean finger width of $w_{f,95\%}$= 66 µm ± 2 µm (s = 6 µm). The interquartile range IQR (between 25. and 75. Quantile) is a good measure for the variation of the finger width. Both groups obtained a comparable IQR of 8 µm (A) and 7 µm (B).

Finger width w_f is influenced by several factors, namely the printing pressure, theadjustment of rollers and printing table, possible register shifts in the second printing step and material tolerances. Thus, the variation of the mean finger width between group A and B might not originate from the ink alone. However, microscopic images of contact fingers from both groups indicate an increased spreading of fingers printed with ink B. A possible explanation could be a considerable difference of the dynamic viscosity of both inks. While ink A has a viscosity η = 358 mPas at a shear rate of $\dot{\gamma}$ = 1000 s^{-1}, the corresponding viscosity of ink B is significantly lower with η = 113 mPas. This difference could be an explanation for the increased ink spreading of ink B on the alkaline textured surface.

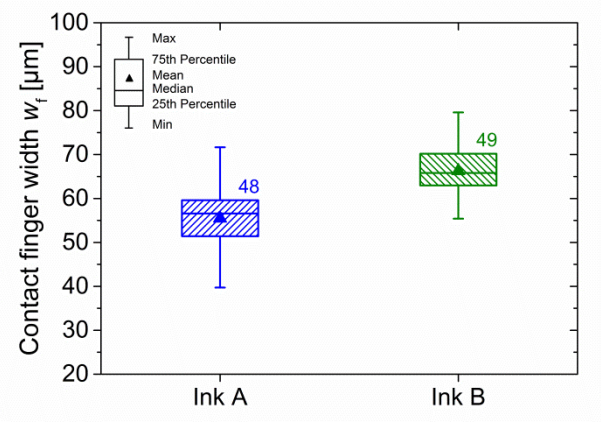

Fig. 5. Mean contact finger width w_f of group A and B.

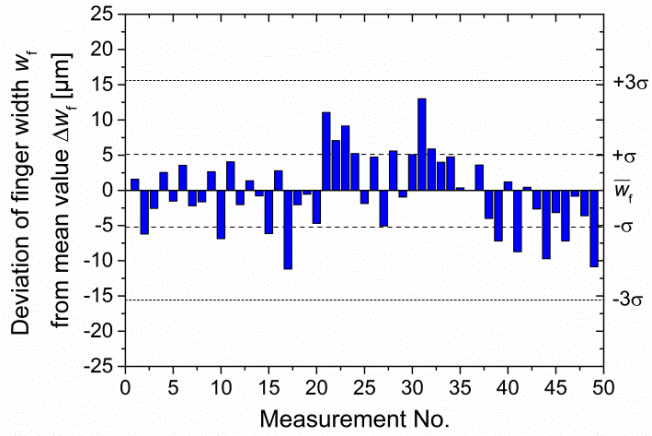

Fig. 4. Deviation of finger width w_f from the mean value (group A)

Fig. 6 illustrates the mean lateral finger resistance R_L of group A and B. Group A achieved $R_{L,95\%}$ = 19.5 ± 4,0 Ω/cm (s = 8,2 Ω/cm), group B obtained $R_{L,95\%}$ = 18.3 ± 1,9 Ω/cm (s = 3,6 Ω/cm). The mean R_L-value of both groups is closely similar at first glance. However, a closer look on the IQR underlines a significantly stronger R_L-variation of group A (IQR = 12,1

Ω/cm) compared to group B (IQR = 3,6 Ω/cm). Comparing microscopic images of contact fingers with both inks does not give an explanation for this finding. It is likely that local variations or restrictions within the measured contact fingers are responsible for the stronger variation of group A. The determined R_L-values are considerably higher than screen-printed contact fingers which usually achieve R_L-values well below below 1 Ω/cm [25]. However, using multiple wires instead of 3 to 5 solder ribbons for interconnection does considerably decrease the effect of R_L on R_s and *FF*. Thus, even a high contact finger resistance does not necessarily lead to a considerable *FF*-loss if an adequate number of wires is used for interconnection [17].

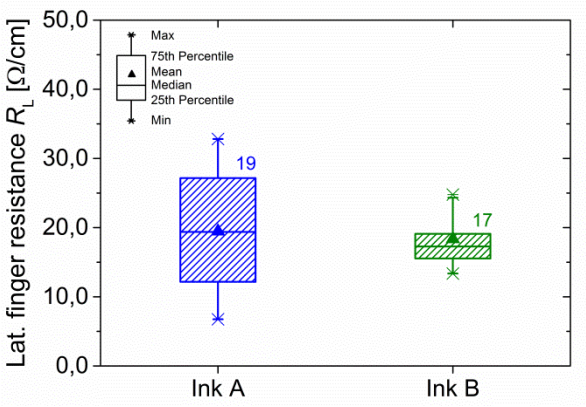

Fig. 6. Lateral finger resistance R_L of group A and B.

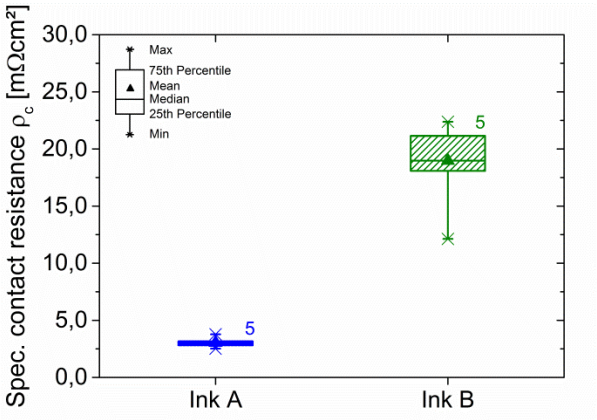

Fig. 7. Specific contact resistance ρ_c of group A and B.

Fig. 7 illustrates the specific contact resistance ρ_c of both inks. A considerable difference is clearly visible. Group A obtained a low mean specific contact resistance of $\rho_{c,95\%} = 3.0 \pm 0.6$ mΩcm² (s = 0.5 mΩcm²) which indicates the capability of this ink formulation to realize a sufficient ohmic contact on the emitter. In contrary, group B revealed a considerably higher mean value of $\rho_{c,95\%} = 19.0 \pm 5{,}2$ mΩcm² (s = 4,1 mΩcm²) and a stronger variation of the individual values. While ink A is optimized for a good contact resistance with a low amount of applied ink, this is not the case for ink B which is intended for thick-film metallization. It is thus likely that ink B is not capable to realize a good contact with a very low finger height as the amount of glass within the diluted paste might not be sufficient.

3.2. Electrical results of busbarless solar cells

Fig. 8 and Fig. 9 show *FF* and conversion efficiency η of the busbarless solar cells – measured with GT/SL –in in dependence of the contact firing peak set temperature T_{FFO}. It is clearly visible that T_{FFO} has a strong impact on the *FF* of the solar cells. Group A achieved mean I-V-values of j_{sc} = 39.5 mA/cm², V_{oc} = 637.2 mV, *FF* = 75.8 % and η = 19.0 % at the best firing temperature of T_{FFO} = 880°C. The best individual solar cell achieved a conversion efficiency of η = 19.4 %. It is possible that a lower peak set firing temperature T_{FFO} < 880 °C might increase the *FF* further. . Group B obtained mean I-V-values of j_{sc} = 34.5 mA/cm², V_{oc} = 638.5 mV, *FF* = 65.9 % and η = 16.5 %, also at T_{FFO} = 880°C. The *FF* of group B is primarily limited by the high specific contact resistance of ink B.

By weighing the wafers before and after the flexo printing and drying step, mean application of only 4.7 mg wet Ag ink per solar on the front side is determined. With the known amount of Ag-particles in the ink (58% for ink A), this gives a very low amount of only 2.7 mg pure silver on each cell. This underlines the potential of this technology to realize a considerable cost reduction for the front side metallization.

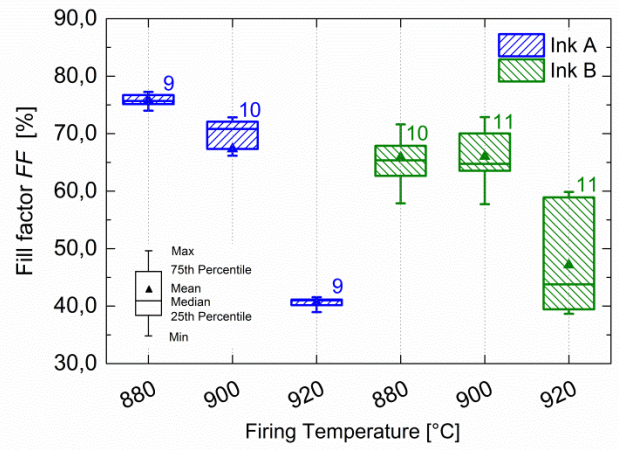

Fig. 8. Fill factor FF of busbarless solar cells of group A and B, fired at three temperatures.

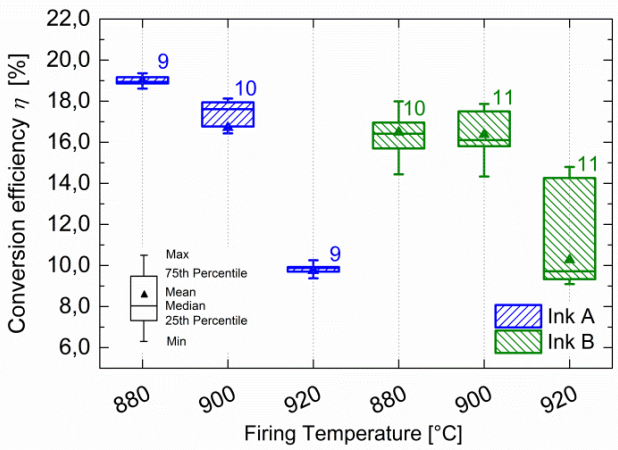

Fig. 9. Conversion efficiency η of group A and B, fired at three temperatures

Summarizing the results, only solar cells of group A obtained promising I-V-results. However, even the *FF* of the best group A at T_{FFO} = 880°C is considerably lower than the typical *FF* of screen printed solar cells. To identify the origin of potential *FF*-losses, a detailed analysis is carried out.

3.3. Fill factor losses related to the front side grid

Generally, *FF* losses on cell level may be caused by leakage currents (expressed by parallel resistance R_p), losses related to series resistance R_s or by recombination losses in the space charge region (SCR). The average area-normalized parallel resistance of the fabricated solar cells is determined with R_p = 63.1 kΩcm² (group A) and R_p = 78.1 kΩcm² (group B). Hence, leakage currents due to a low R_P can be neglected.

R_s-related *FF* losses can origin from emitter, base or metallization. The characteristics of the wafer material and the screen-printed Al BSF are well known and can thus be excluded. Thus, the series resistance contribution of the grid $r_{s,grid}$ or the metal-semiconductor contact $r_{s,contact}$ remains as the potential source for the between metal and emitter (front side metallization remains as the possible source for above-average *FF* losses. Furthermore, *FF* losses due to local transition resistances R_{trans} between fingers and wires during the GT/SL-measurement have to be taken into account.

To estimate the impact of $r_{s,grid}$ and $r_{s,contact}$ on the *FF* of the solar cells, a calculation is carried out according to [26–29]. It is assumed that all 100 contact fingers of the flexo-printed front side metallization would obtain the determined mean lateral finger resistance R_L and specific contact resistance ρ_c. As $r_{s,grid}$ strongly depends on the number of wires used for measurement/interconnection, the calculation is carried out for different interconnection scenarios 18, 30 and 38 wires with a diameter of d_{wire} = 200 µm.

$r_{s,contact}$ depends on the ink, firing conditions and the properties of the emitter and stays constant for different amounts of wires.

Table 1: Calculated R_s-contribution and FF-loss ΔFF_{tot} related to the front side metallization for group A and B

Group	**R_L [Ω/cm]**	**ρ_c [mΩcm²]**	**# of wires**	**$\Delta r_{s,grid}$ [Ωcm²]**	**$\Delta r_{s,contact}$ [Ωcm²]**	**$\Delta r_{s,tot}$ [Ωcm²]**	**ΔFF_{tot} [%$_{abs}$]**
A	19.5	3.0	18	0.18	0.09	0.27	-1.54
			30	0.06		0.15	-0.86
			38	0.04		0.13	-0.74
B	18.3	19.0	18	0.17	0.46	0.63	-3.59
			30	0.06		0.52	-2.96
			38	0.04		0.50	-2.85

The calculation shows that the total series resistance contribution of the grid strongly depends on the amount of wires used for measurement/interconnection. The results further show that only ink A achieved a sufficiently low contact resistance. With respect to the *FF*, more wires

are obviously beneficial for flexo-printed solar cells due to the high R_L of the contact fingers. However, using more wires for solar cell interconnection also increases shading losses on module level. Thus, using more but thinner wires could be a solution to decrease *FF*-losses and avoid additional j_{sc}-losses in parallel.

Further *FF*-losses could origin from recombination losses in the SCR due to the front side metallization. Dark saturation current density j_{02} is a measure for such recombination losses. Ideally, j_{02} can be calculated using the dark IV curve of solar cells as fitting to the dark IV curve facilitates to distinguish j_{02} and R_s [30]. Thus, dark saturation current density j_{02} is estimated by fitting the two-diode-model to the illuminated I-V-curve of the solar cells [30]. Using this method, a mean dark saturation current density of j_{02} = 60 nA/cm² is calculated for solar cells of group A. This value is considerably higher than what is typically expected for screen-printed solar cells on the same wafer material. This could be an indication for recombination losses in the SCR due to the front side metallization. Yet, to make a clear statement about the presence of such losses, this phenomenon should be investigated using the dark I-V-curves of the solar cells.

3.4. Losses related to the wire interconnection

As the GT/SL-measurement system focuses on the measurement of the bare busbarless solar cell, any impact of the wires on *FF* and j_{sc} is obviously not considered in the I-V-results. However, the number of wires used for interconnection does strongly affect j_{sc}-losses related to shading and *FF*-losses related to series resistance on module level. R_s-contribution of the interconnection wires $r_{s,wire}$ and FF-losses are calculated for 18, 30 and 38 wires with ρ_{wire} = 1.68 µΩcm according to [27,28]. A further unknown R_s-contribution is presumably induced by local transition resistances between fingers and wires R_{trans}. The quantity of R_{trans} probably strongly depends on local inhomogeneities of the contact fingers and tolerances of the wafer surface (i.e. saw marks). Thus, the resulting series resistance contribution $r_{s,trans}$ might have a considerable impact on the global *FF* of the module. However, it is currently not possible to quantify $r_{s,trans}$ properly. J_{sc}-losses are in good approximation proportional to the fraction of shading caused by the wires, if additional reflection and absorption gains and losses due to encapsulation, glass and backsheet are neglected. This j_{sc}-loss can be calculated with an assumed photo-generated current density j_{ph} = 40 mA/cm² and percentage of shading on the front side $A_{sh\%,grid}$. The shading impact on j_{sc} is calculated for 18, 30 and 38 wires with a wire diameter of d_{wire} = 200 µm and an effective shading width of 59 % [31] due to the round wire geometry. Reflection and absorption effects due to module encapsulation, glass and backsheet

on j_{sc} are not considered in the calculation. *Table 2* shows the calculated FF- and j_{sc}-loss for an interconnection with 18, 30 or 38 wires and an effective wire shading of d_{eff} = 59 %.

Table 2: Calculated FF- and j_{sc}-loss of the wire interconnection using 18, 30 or 38 wires

# of wires	$\Delta r_{s,wire}$ [Ωcm²]	ΔFF_{wire} [%$_{abs}$]	$A_{sh,wire}$ [%]	Δj_{sc} [mA/cm²]
18	0.38	-3.71	1.36	-0.54
30	0.23	-2.17	2.27	-0.91
38	0.18	-1.77	2.87	-1.15

Finally, a small voltage loss of approx. ΔV_{oc} = 0.5 mV can be assumed which originates from the voltage measurement characteristics of GT/SL.

3.5. Calculated offset between the IV-measurement of solar cells and module

Due to the characteristics of the GT/SL-measurement, one can expect a considerable offset of IV-results on cell and module level. The quantity of this offset is estimated for the fabricated solar cells of group A by calculating the total offset in conversion efficiency Δη from the expected difference in j_{sc}, V_{oc} and *FF*. With respect to j_{sc}, the additional shading of the wires is considered. The *FF*-offset incorporates the series resistance contribution of the wires and the impact of the wire number on the finger segment length in between two wires. The results of the calculation are shown in *Table 3*.

Table 3: Calculated offset of IV-values for group A between a measurement on cell level using GT/SL and IV-measurement of the same solar cells after multi-wire interconnection

No. of wires	I-V-Offset between Grid^{TOUCH} -measurement and wire-interconnected solar cells			
	Δj_{sc} [mAcm²]	ΔV_{oc} [mV]	ΔFF [%$_{abs}$]	Δη [%$_{abs}$]
18	-0.54	-0.50	-2.85	-0.92
30	-0.91	-0.50	-1.31	-0.71
38	-1.15	-0.50	-0.91	-0.72

The results show that a considerable offset has to be considered when comparing the IV-results of the GT/SL-measurement to the IV-results of a module using the same cells. Due to the high lateral finger resistance of the flexo-printed front side grid, this offset is particularly high with regard to the fabricated solar cells. Additionally, the different mechanism of the finger-wire-interconnection within the GT/SL-measurement (mechanical pressure) and the module (wire-bonding interconnection) has to be considered. However, the quantity of the

resulting transistion resistance and the possible impact on the *FF*-offset is currently unknown and thus not considered within this work.

3.6. Characterization of the mini-module

The measured I-V-results of the interconnected and encapsulated mini-module as well as the IV-results of the two individual solar cells (GT/SL-measurement) are shown in Table 4.

Table 4: I-V-results of the mini-module and the two individual solar cells (GT/SL-measurement)

	I_{sc} [A]	**V_{oc} [mV]**	**FF [%]**	**η [%]**
Solar cell 1[a]	9.59	640	77.3	19.4
Solar cell 2[a]	9.61	640	76.9	19.3
Mini-module[b]	9.21	1273	67.5	15.8
Absolute CTM-loss	-0.4 A	-7 mV	-9.6 $\%_{abs}$	-3.6 $\%_{abs}$
Relative CTM-loss	-4.2 %	-0.5 %	-12.5 %	-18.6 %

[a]Grid[TOUCH]-measurement: j_{sc}-values calculated without shading of wires, *FF* measured with 30 wires

[b]I-V-measurement of interconnected and encapsulated cells (18 wires) with black mask; Aperture module efficiency related to measurement with black mask (Mask opening 318 mm x 158 mm)

The I-V-results reveal an average cell-to-module (CTM) loss of $\Delta\eta \approx$ -3.6 $\%_{abs}$ which is primarily caused by a considerable *FF*-loss. To explain this CTM loss, several aspects have to be taken into account:

- An offset of $\Delta\eta \approx 0.92\ \%_{abs}$ can be expected due to the measurement characteristics of GT/SL as shown in section 3.5
- Ohmic losses of the crosslinkin ribbons further contribute to *FF*-losses
- Typical CTM-losses as described in [32] have to be considered
- Locally increased transition resistances due to low-quality wire-bonding interconnections or areas with completely defective interconnection might contribute substantially to *FF*-losses within the module

The first three causes do not explain the total CTM-loss. Thus it is likely that the wire-bonding interconnection might contribute significantly to the *FF*-loss within the module. To investigate the quality of the wire-bonding interconnection as well as further sources of *FF*-losses, an EL-measurement of the module is carried out (Fig. 10). Dark areas in the EL-image represent regions with a high local series resistance.

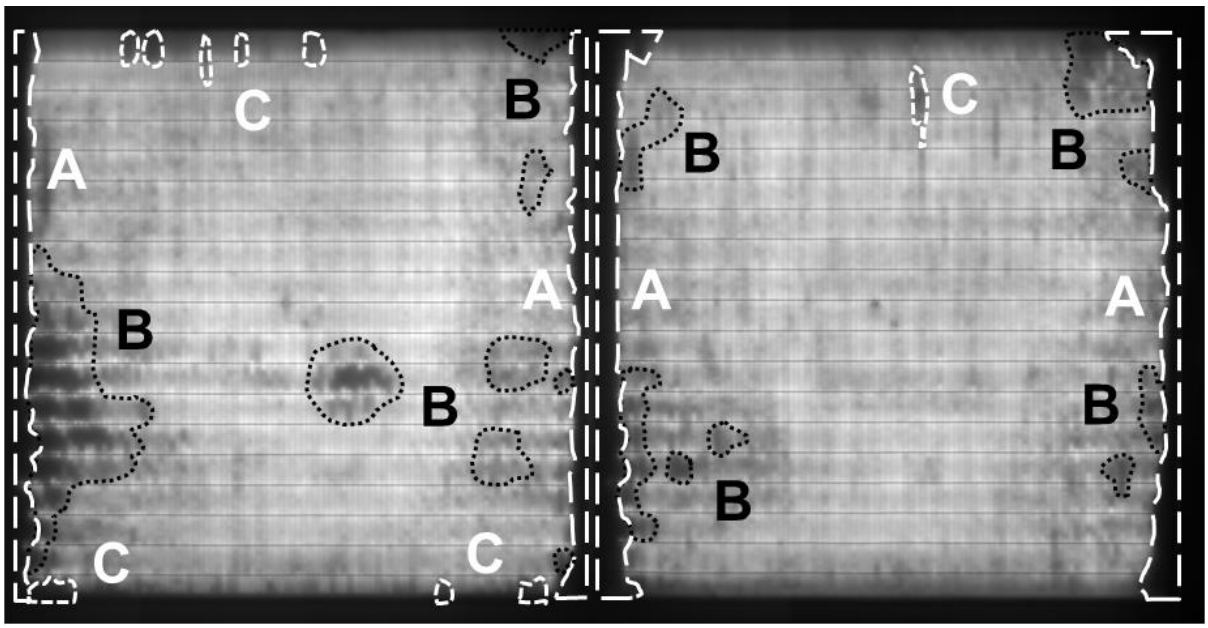

Fig. 10. EL-measurement of the demonstrator module. The following defects are identified: A) Failed interconnection between wire and contact fingers, B) Areas with high series resistance, most likely related to the front side grid, C) Areas of high series resistance probably due to defect wire-bonding interconnections.

Along the edge of the solar cells, failed interconnections between wire electrodes and contact fingers are identified (A). Some regions (B) within the active area of the solar cells reveal a considerably higher series resistance which could origin from an inhomogeneous printing quality. Such inhomogeneities can cause non-visible finger restrictions, local interruptions or areas with a high contact resistance. As the impact of the finger resistance R_L on the *FF* increases with a decreasing amount of wires, such regions might have a stronger impact in the module (18 wires) compared to the GT/SL-measurement (30 wires). Occasionally, local defective interconnections between fingers and wire as previously described in [33,34] can be found (C). A detailed investigation of the identified defects with special focus on the wire-bonding interconnection will be one of the main goals of further studies.

4. Conclusion

Within the first experiment, two types of Ag-ink have been printed and evaluated with respect to optical and electrical properties of the front side grid. Ink A which is optimized for flexo printing on Si solar cells obtained a low specific contact resistance of ρ_c = 3.0 ± 0.6 mΩcm². Ink B, a diluted screen printing Ag-paste, achieved considerably worse results of ρ_c = 19.0 ± 5.2 mΩcm². This might origin from the incapability of ink B to enable a good ohmic contact on the emitter with a very small finger height. Both inks obtained a similar mean lateral finger resistance between 18.3 and 19.5 Ω/cm. Busbarless Al-BSF solar cells with flexo-printed front side metallization have been fabricated and measured using a Pasan Grid^{TOUCH} in a Spot^{LIGHT} measurement device. The best group of solar cells achieved an average conversion efficiency of $\eta_{\varnothing}$ = 19.0 % (best individual solar cell η_{max} = 19.4 %). Only a very low amount of 4.7 mg of wet ink respectively 2.7 mg of pure silver has been applied on the front side of the solar cells. A fully functional mini-module has been fabricated by interconnecting the best two solar cells of group A with 18 wires via SmartWire Connection Technology. However, I-V-results of the mini-module revealed considerable cell-to-module losses. These losses can be partly explained by a certain offset due to the measurement characteristics of Grid^{TOUCH}, ohmic losses of the crosslinking ribbons and further typical CTM losses of the encapsulated module. Further losses are most likely caused by local transition resistances or defective areas of the wire-bonding interconnection. An EL-measurement of the mini-module revealed such partly defective contacts as well as areas with high series resistance within the front side grid. Further research activities must focus on an optimization of the printing process, the ink formulation, the amount and diameter of wires used for SWCT interconnection as well as an optimization of the wire-bonding interconnections. In summary, we demonstrate the ability of rotational flexographic printing for the front side metallization of busbarless solar cells with good electrical results and very low silver consumption. This demonstrates the very high potential for cost savings using flexographic printing processes.

Acknowledgements

This work was partly supported by the German Federal Ministry of Education and Research (BMBF) within the funding program Photonics Research Germany under the contract number 13N13512 (Rock-Star). The authors further thank Somont GmbH, Meyer Burger AG,

ContiTech Elastomer-Beschichtungen GmbH as well as Johannes Greulich and Tobias Fellmeth for the support of this work.

5. References

[1] Hörteis M, Richter P, Glunz SW. Improved Front Side Metallization by Aerosol Jet Printing of Hotmelt Inks. In: WIP, editor. *Proc. of the 23rd EUPVSEC*; 2008, p. 1402–5.

[2] Hörteis M, Mette A, Richter P, Fidorra F, Glunz S. Further progress in metal aerosol jet printing for front side metallization of silicon solar cells. In: WIP, editor. *Proc. of the 22nd EUPVSEC*; 2007, p. 1039–42.

[3] Ebong A, Rounsaville B, Cooper IB, Tate K, Rohatgi A, Glunz S, Horteis M, Met A, Gundermann M, Xjet. High efficiency silicon solar cells with ink jetted seed and plated grid on high sheet resistance emitter. In: IEEE, editor. *35th IEEE Photovoltaic Specialists Conference*; 2010, p. 1363–7.

[4] Stüwe D, Mager D, Biro D, Korvink JG. Inkjet Technology for Crystalline Silicon Photovoltaics. *Adv. Mater.* 2014:1–28, doi:10.1002/adma.201403631.

[5] Hörteis M, Bartsch J, Binder S, Filipovic A, Merkel J, Radtke V, Glunz SW. Electrical properties of fine line printed and light-induced plated contacts on silicon solar cells. *Prog. Photovolt: Res. Appl.* 2010:n/a, doi:10.1002/pip.938.

[6] Olweya S, Kalio A, Kraft A, Deront E, Filipovic A, Bartsch J, Glatthaar M. Fine-line Silver Pastes for Seed Layer Screen Printing with Varied Glass Content. *Energy Procedia* 2013;43:37–43, doi:10.1016/j.egypro.2013.11.086.

[7] Hashimoto K, Ouchi M, Nakamura N, Kobayashi E, Watabe Y. Low Cost Module with Heterojunction Solar Cells Applied Gravure Offset Printing and Multi-Wire Technologies. In: WIP, editor. *Proc. of the 28th EUPVSEC*; 2013, p. 1073–6.

[8] Deganello D, Cherry J, Gethin D, Claypole T. Patterning of micro-scale conductive networks using reel-to-reel flexographic printing. *Thin Solid Films* 2010;518:6113–6, doi:10.1016/j.tsf.2010.05.125.

[9] Deganello D, Cherry J, Gethin D, Claypole T. Impact of metered ink volume on reel-to-reel flexographic printed conductive networks for enhanced thin film conductivity. *Thin Solid Films* 2012;520:2233–7, doi:10.1016/j.tsf.2011.08.050.

[10] Krebs FC, Fyenbo J, Jørgensen M. Product integration of compact roll-to-roll processed polymer solar cell modules: methods and manufacture using flexographic

printing, slot-die coating and rotary screen printing. *J. Mater. Chem.* 2010;20:8994–9001, doi:10.1039/c0jm01178a.

[11] Wang Z, Winslow R, Madan D, Wright PK, Evans JW, Keif M, Rong X. Development of MnO2 cathode inks for flexographically printed rechargeable zinc-based battery. *Journal of Power Sources* 2014;268:246–54, doi:10.1016/j.jpowsour.2014.06.032.

[12] Kwak MK, Shin KH, Yoon EY, Suh KY. Fabrication of conductive metal lines by plate-to-roll pattern transfer utilizing edge dewetting and flexographic printing. *Journal of Colloid and Interface Science* 2010;343:301–5, doi:10.1016/j.jcis.2009.11.003.

[13] Frey M, Clement F, Dilfer S, Erath D, Biro D. Front-side Metalization By Means Of Flexographic Printing. *Energy Procedia* 2011:581–6.

[14] Thibert S, Jourdan J, Bechevet B, Mialon S, Beneventi D, Chaussy D, Reverdy-Bruas N. Flexographic Process for Front Side Metallization of Silicon Solar Cell. In: WIP, editor. *Proc. of the 28th EUPVSEC*; 2013, p. 1013–6.

[15] Thibert S, Chaussy D, Beneventi D, Reverdy-Bruas N, Jourdan J, Bechevet B, Mialon S. Silver ink experiments for silicon solar cell metallization by flexographic process. In: *38th IEEE PVSC*; 2012, p. 2266–70.

[16] Lorenz A, Kalio A, Barnes Hofmeister T, Kraft A, Bartsch J, Clement F, Reinecke H, Biro D. Developing a high throughput printing technology for silicon solar cell front side metallisation using flexography. *J. Print Media Technol. Res.* 2014:227–40, doi:10.14622/JPMTR-1408.

[17] Söderström T, Papet P, Yao Y, Ufheil J. *SmartWire Connection Technology*; 2014.

[18] Braun S, Micard G, Hahn G. Solar Cell Improvement by using a Multi Busbar Design as Front Electrode. *Energy Procedia* 2012;27:227–33, doi:10.1016/j.egypro.2012.07.056.

[19] Lorenz A, Senne A, Rohde J, Kroh S, Wittenberg M, Krüger K, Clement F, Biro D. Evaluation of Flexographic Printing Technology for Multi-busbar Solar Cells. *Energy Procedia* 2015;67:126–37, doi:10.1016/j.egypro.2015.03.296.

[20] Lorenz A, Kalio A, Hofmeister GT, Nold S, Kraft A, Bartsch J, Wolf A, Dreher M, Clement F, Biro D. Flexographic Printing – High Throughput Technology for Fine Line Seed Layer Printing on Silicon Solar Cells. In: WIP, editor. *Proc. of the 28th EUPVSEC*; 2013, p. 1017–23.

[21] Kontermann S, Hörteis M, Ruf A, Feo S, Preu R. Spatially resolved contact-resistance measurements on crystalline silicon solar cells. *Phys. Status Solidi (a)* 2009:NA, doi:10.1002/pssa.200925077.

[22] Pysch D, Mette A, Filipovic A, Glunz SW. Comprehensive analysis of advanced solar cell contacts consisting of printed fine-line seed layers thickened by silver plating. *Prog. Photovolt: Res. Appl.* 2009;17:101–14, doi:10.1002/pip.855.

[23] Hermans JP, Papet P, Pacheco K, Brok W, Strahm B, Rochat J, Söderström T, Yao Y. Advanced metallization concepts by inkjet printing. In: WIP, editor. *Proc. of the 29th EUPVSEC*; 2014, p. 518–22.

[24] Meyer Burger AG. *The GridTouch contacting system: Article PV Production Annual 2014*. Available at: http://www.meyerburger.com/fileadmin/user_upload/meyerburger.com/Downloads/Publikationen/Dokumente/2014_PV_Annual_GridTouch.pdf; 2014 [accessed 10.12.2015].

[25] Lorenz A, Strauch T, Demant M, Fellmeth T, Barnes Hofmeister T, Linse M, Dannenberg T, Seiffe J, Clement F, Biro D, Reinecke H, Preu R. Impact of Texture Roughness on the Front-Side Metallization of Stencil-Printed Silicon Solar Cells. *IEEE J. Photovoltaics* 2015;5:1237–44, doi:10.1109/JPHOTOV.2015.2416916.

[26] Fellmeth T, Clement F, Biro D. Analytical Modeling of Industrial-Related Silicon Solar Cells. *IEEE J. Photovoltaics* 2014;4:504–13, doi:10.1109/JPHOTOV.2013.2281105.

[27] Fellmeth T. *Silicon Solar Cells for the Application in Low Concentrator Systems-Development and Characterization*. Dissertation, Eberhard Karls Universität Tübingen. Tübingen; 2014.

[28] Mette A. *New concepts for front side metallization of industrial silicon solar cells*. Dissertation, Albert-Ludwigs-Universität. Freiburg; 2007.

[29] Goetzberger A, Knobloch J, Voss B. *Crystalline silicon solar cells.* 3rd ed. Chichester, UK: Wiley; 1998.

[30] Greulich J, Glatthaar M, Rein S. Fill factor analysis of solar cells' current-voltage curves. *Prog. Photovolt: Res. Appl.* 2010;18:511–5, doi:10.1002/pip.979.

[31] Witteck R, Hinken D, Schulte-Huxel H, Vogt MR, Muller J, Blankemeyer S, Kontges M, Bothe K, Brendel R. Optimized Interconnection of Passivated Emitter and Rear Cells by Experimentally Verified Modeling. *IEEE J. Photovoltaics* 2016;6:432–9, doi:10.1109/JPHOTOV.2016.2514706.

[32] Haedrich I, Eitner U, Wiese M, Wirth H. Unified methodology for determining CTM ratios: Systematic prediction of module power. *Solar Energy Materials and Solar Cells* 2014;131:14–23, doi:10.1016/j.solmat.2014.06.025.

[33] Papet P, Andreetta L, Lachenal D, Wahli G, Meixenberger J, Legradic B, Frammelsberger W, Bätzner D, Strahm B, Yao Y, Söderström T. New Cell Metallization

Patterns for Heterojunction Solar Cells Interconnected by the Smart Wire Connection Technology. *Energy Procedia* 2015;67:203–9, doi:10.1016/j.egypro.2015.03.039.

[34] Yao Y, Papet P, Hermans J, Soderstrom T, Mehlich H, Konig M, Waltinger A, Habermann D, Richter A. Module integration of solar cells with diverse metallization schemes enabled by SmartWire Connection Technology. In: *2015 IEEE 42nd Photovoltaic Specialists Conference (PVSC)*, p. 1–5.